A BEM for transient coupled thermoelastic crack analysis of homogeneous/functionally graded bimaterials

Alexander Ekhlakov[1,2*], Oksana Khay[1,3], Chuanzeng Zhang[1]

[1] Department of Civil Engineering, University of Siegen, Paul-Bonatz-Str. 9-11, D-57076 Siegen, Germany
[2] Faculty of Architecture and Civil Engineering, RheinMain University of Applied Sciences, Kurt-Schumacher-Ring 18, D-65197 Wiesbaden, Germany
[3] Pidstryhach Institute for Applied Problems of Mechanics and Mathematics NASU, 3b Naukova Str., 79060 L'viv, Ukraine
* Corresponding author: alexander.ekhlakov@hs-rm.de

Abstract A transient coupled thermoelastic analysis of two-dimensional, isotropic and linear elastic bimaterials, which are composed of a functionally graded (FG) layer attached to a homogeneous substrate, subjected to thermal shock is investigated. For this purpose, a boundary element method (BEM) for linear coupled thermoelasticity is developed. The material properties of the FG layer are assumed to be continuous functions of the spatial coordinates. The boundary-domain integral equations are derived by using the fundamental solutions of linear coupled thermoelasticity for the corresponding isotropic, homogeneous and linear thermoelastic solids in the Laplace-transformed domain. For the numerical solution, a collocation method with piecewise quadratic approximation is implemented. Numerical results for the dynamic stress intensity factors are presented and discussed.

Keywords Functionally graded materials, Homogeneous/functionally graded bimaterials, Transient linear coupled thermoelasticity, Boundary element method, Dynamic stress intensity factors

1. Introduction

Functionally graded materials (FGMs) represent a new generation of high-performance composite materials formed by continuously variable composition of the constituents over volume [1]. They possess many superior mechanical, thermal, corrosion-resistant and wear-resistant properties in comparison to the conventional composite materials. Therefore, in recent years FGMs have received an increasing research interest in materials and engineering sciences. An important application area of FGMs is in the thermal barrier coating technology, where a functionally graded (FG) layer is deposited on a homogeneous substrate. Thermoelastic fracture analysis of FG coated materials and structures is of particular importance to their thermal and mechanical integrity, reliability and durability in novel engineering applications. Such analysis may provide a fundamental understanding of and a deep insight into the failure mechanisms of FG coated materials and structures, which may aid in their design, optimization and applications. Due to the high mathematical complexity of the corresponding dynamic thermoelastic problems for non-homogeneous FGMs, analytical methods can be obtained only for very simple geometry and loading conditions. In general cases, numerical and experimental methods have to be applied to fracture and fatigue analysis in FG coated materials and structures subjected to thermal shock loading conditions.

In this paper, a boundary element method (BEM) for transient thermoelastic crack analysis in two-dimensional (2-D), isotropic and linear thermoelastic bimaterials consisting of an FG coating layer attached to a homogeneous substrate under thermal shock is developed. The FG/homogeneous bimaterials are modeled by using a sub-domain technique [2]. The bimaterial system is divided into a homogeneous and a non-homogeneous sub-domain along the interface. The equations of motion and the thermal balance equation constitute the governing equations of the transient linear coupled thermoelasticity. The Laplace-transform technique is applied to eliminate the time-dependence in the governing equations. A boundary-domain integral equation representation is derived from the generalized Betti's reciprocal theorem for FGMs in conjunction with the fundamental solutions for

homogeneous and linear thermoelastic solids. The boundary-domain integral equations (BDIEs) are obtained for the unknown mechanical and thermal fields and then applied to each sub-domain and the continuity conditions are employed on the interface boundary. The BDIEs for the FG layer contain domain integrals, which describe the material's non-homogeneity. A crucial point of the numerical solution procedure is how to evaluate the domain integrals without discretization of the non-homogeneous sub-domain into internal cells. In this analysis, the domain integrals are transformed into boundary integrals over the global boundary by using the radial integration method (RIM) [3, 4]. For the homogeneous and linear elastic substrate, only boundary integrals need to be considered in the boundary integral equations. A collocation method is implemented for the spatial discretization. The final time-dependent solutions are obtained by using the Stehfest's algorithm [5] for the inverse Laplace-transform. Numerical results are presented and discussed to demonstrate the accuracy and efficiency of the proposed BEM as well as the effects of the material gradation and thermo-mechanical coupling on the dynamic stress intensity factors (SIFs).

2. Problem statement

Let us consider isotropic and linear thermoelastic bimaterials in a 2-D domain, which are composed of an FG layer attached to a homogeneous substrate. The FG/homogeneous bimaterials are modeled by using a sub-domain technique [2]. The bimaterial system is divided into a homogeneous $\Omega^{(0)}$ and a non-homogeneous sub-domain $\Omega^{(1)}$ along the interface. The material properties of the FG layer such as the mass density $\tilde{\rho}_1(\mathbf{x})$, the Young's modulus $E_1(\mathbf{x})$, the thermal conductivity $k_1(\mathbf{x})$, the specific heat $c_1(\mathbf{x})$ and the linear expansion coefficient $\alpha_1(\mathbf{x})$ are assumed to be continuous functions of the Cartesian coordinates, while the Poisson's ratio ν_1 and the material parameters of the homogeneous substrate, which are denoted by a subscript zero, are taken as constant. In this case, the elasticity tensor can be written as

$$c_{ijkl}^{(0)} = \mu_0 c_{ijkl}^{(0)0}, \qquad c_{ijkl}^{(1)}(\mathbf{x}) = \mu_1(\mathbf{x}) c_{ijkl}^{(1)0} \tag{1}$$

with

$$\mu_0 = \frac{E_0}{2(1+\nu_0)}, \qquad \mu_1(\mathbf{x}) = \frac{E_1(\mathbf{x})}{2(1+\nu_1)}, \qquad c_{ijkl}^{(n)0} = \frac{2\nu_n}{1-2\nu_n}\delta_{ij}\delta_{kl} + \delta_{ki}\delta_{lj} + \delta_{kj}\delta_{li}, \qquad n = 0,1,$$

where μ_n is the shear modulus and δ_{ij} is the Kronecker delta symbol. The relation between the stresses $\sigma_{ij}^{(n)}(\mathbf{x},t)$ and the displacements $u_{k,l}^{(n)}(\mathbf{x},t)$ with the consideration of the temperature changes $\theta^{(n)}(\mathbf{x},t)$ is defined by the Duhamel-Neumann constitutive equations

$$\sigma_{ij}^{(n)}(\mathbf{x},t) = c_{ijkl}^{(n)}(\mathbf{x}) u_{k,l}^{(n)}(\mathbf{x},t) - \gamma_n(\mathbf{x})\theta^{(n)}(\mathbf{x},t)\delta_{ij}, \qquad n = 0,1, \tag{2}$$

where the stress-temperature modulus is given by $\gamma_n = E_n\alpha_n/(1-2\nu_n)$. In the absence of body forces and heat sources, the governing equations in transient linear coupled thermoelasticity are given by the equations of motion and the thermal balance equations [6]

$$\sigma_{ij,j}^{(n)}(\mathbf{x},t) - \tilde{\rho}_n(\mathbf{x})\ddot{u}_i^{(n)}(\mathbf{x},t) = 0, \tag{3}$$

$$\left(k_n(\mathbf{x})\theta_{,i}^{(n)}(\mathbf{x},t)\right)_{,i} - \tilde{\rho}_n(\mathbf{x})c_n(\mathbf{x})\dot{\theta}^{(n)}(\mathbf{x},t) - k_n(\mathbf{x})\eta_n(\mathbf{x})\dot{u}_{k,k}^{(n)}(\mathbf{x},t) = 0, \tag{4}$$

where $\eta_n = \gamma_n T_0 / k$ and T_0 is the reference temperature. Unless otherwise stated, the conventional summation rule over double indices is implied, $n = 0,1$ and other Latin indices take the values of 1

and 2. From the mathematical point of view, the governing equations are the coupled partial differential equations with variable coefficients for the FG sub-domain $\Omega^{(1)}$. A measure of the thermo-mechanical coupling due to the dilatational term $\eta_n \dot{u}_{k,k}^{(n)}$ in Eq. (4) is defined by a dimensionless coupling parameter [6, 7]

$$\delta_n = \frac{(1+\nu_n)}{(1-\nu_n)(1-2\nu_n)} \frac{E_n \alpha_n^2 T_0}{\tilde{n}_n c_n}, \tag{5}$$

that equals zero for an uncoupled problem.

The following essential and natural boundary conditions for the mechanical and thermal quantities are prescribed as

$$\begin{aligned} u_i^{(n)}(\mathbf{x},t) &= \tilde{u}_i^{(n)}(\mathbf{x},t), \quad \mathbf{x} \in \Gamma_u^{(n)}, & \theta^{(n)}(\mathbf{x},t) &= \tilde{\theta}^{(n)}(\mathbf{x},t), \quad \mathbf{x} \in \Gamma_\theta^{(n)}, \\ t_i^{(n)}(\mathbf{x},t) &= \tilde{t}_i^{(n)}(\mathbf{x},t), \quad \mathbf{x} \in \Gamma_t^{(n)}, & q^{(n)}(\mathbf{x},t) &= \tilde{q}^{(n)}(\mathbf{x},t), \quad \mathbf{x} \in \Gamma_q^{(n)}, \end{aligned} \tag{6}$$

where $t_i^{(n)}$ and $q^{(n)}$ represent the traction vector and the heat flux defined by

$$t_i^{(n)}(\mathbf{x},t) = \sigma_{ij}^{(n)}(\mathbf{x},t) n_j(\mathbf{x}), \qquad q^{(n)}(\mathbf{x},t) = -k_n(\mathbf{x}) \theta_{,i}^{(n)}(\mathbf{x},t) n_i(\mathbf{x}).$$

Here, $n_i(\mathbf{x})$ denotes the components of the outward unit normal vector, $\Gamma_u^{(n)}$ and $\Gamma_t^{(n)}$ are the parts of the external boundary $\Gamma^{(n)} = \Gamma_u^{(n)} \cup \Gamma_t^{(n)}$, $\Gamma_u^{(n)} \cap \Gamma_t^{(n)} = \varnothing$, in which the displacements $\tilde{u}_i^{(n)}$ and the tractions $\tilde{t}_i^{(n)}$ are given, respectively; $\Gamma_\theta^{(n)}$ and $\Gamma_q^{(n)}$ are the parts of the boundary $\Gamma^{(n)} = \Gamma_\theta^{(n)} \cup \Gamma_q^{(n)}$, $\Gamma_\theta^{(n)} \cap \Gamma_q^{(n)} = \varnothing$ with the specified temperature $\tilde{\theta}^{(n)}$ and the heat flux $\tilde{q}^{(n)}$, respectively. The crack-faces are assumed to be free of mechanical and thermal loadings

$$t_i^{(n)}(\mathbf{x},t) = 0, \quad \mathbf{x} \in \Gamma_c, \qquad q^{(n)}(\mathbf{x},t) = 0, \quad \mathbf{x} \in \Gamma_c, \tag{7}$$

where $\Gamma_c = \Gamma_c^+ \cup \Gamma_c^-$ represents the upper and lower crack-faces. The continuity conditions on the interface are prescribed as

$$\begin{aligned} u_i^{(0)}(\mathbf{x},t) &= u_i^{(1)}(\mathbf{x},t), & \theta^{(0)}(\mathbf{x},t) &= \theta^{(1)}(\mathbf{x},t), \quad \mathbf{x} \in \Gamma^{(01)}, \\ t_i^{(0)}(\mathbf{x},t) &= -t_i^{(1)}(\mathbf{x},t), & q^{(0)}(\mathbf{x},t) &= -q^{(1)}(\mathbf{x},t), \quad \mathbf{x} \in \Gamma^{(01)}. \end{aligned} \tag{8}$$

The initial conditions are given by

$$u_i(\mathbf{x},t) = \dot{u}_i(\mathbf{x},t) = 0, \quad \theta(\mathbf{x},t) = 0 \qquad \text{for} \quad t \le 0. \tag{9}$$

Applying the Laplace-transform to Eqs. (3) and (4) and substituting Eqs. (1) and (2) yield

$$\begin{aligned} & c_{ijkl}^{(n)0} \left(\mu_n \bar{u}_{k,lj}^{(n)} + \mu_{,j}^{(n)} \bar{u}_{k,l}^{(n)} \right) - \left(\gamma_n \bar{\theta}_{,i}^{(n)} + \gamma_{n,i} \bar{\theta}^{(n)} \right) - \rho^{(n)} p^2 \bar{u}_i^{(n)} = 0, \\ & \bar{\theta}_{,ii}^{(n)} + \frac{k_{n,i}}{k_n} \bar{\theta}_{,i}^{(n)} - \beta_n^2 \bar{\theta}^{(n)} - \eta_n p \bar{u}_{k,k}^{(n)} = 0, \end{aligned} \tag{10}$$

where a superimposed bar over a quantity denotes the Laplace-transformed quantity, p is the Laplace-transform parameter, κ_n 戴 $k_n / \tilde{n}_n c_n$ is the thermal conductivity and $\beta_n^2 = p / \kappa_n$.

Integral representations of the displacements and the temperature at an arbitrary point of the domain are derived from the generalized Betti's reciprocal theorem in conjunction with the fundamental solutions of the Laplace-transformed linear coupled thermoelasticity for a homogeneous solid [6, 8, 9]. By moving the observation point to the boundary $\mathbf{x} \in \Gamma^{(n)}$ or keeping it in the domain $\mathbf{x} \in \Omega^{(n)}$ the

following system of boundary-domain integral equations (BDIEs) for the mechanical and thermal fields at the boundary and interior points is obtained as

$$\begin{aligned}
&\overline{u}_j^{(n)}(\mathbf{x},p)+\int_\Gamma\left[\overline{T}_{ij}(\mathbf{x},\mathbf{y},p)\overline{u}_i^{(n)}(\mathbf{y},p)-\frac{1}{\tilde{E}(\mathbf{y})\tilde{\alpha}(\mathbf{y})}\overline{U}_{ij}(\mathbf{x},\mathbf{y},p)\overline{t}_i^{(n)}(\mathbf{y},p)\right]d\Gamma\\
&\quad-\kappa_0\int_\Gamma\left[\overline{Z}_j(\mathbf{x},\mathbf{y},p)\overline{\theta}^{(n)}(\mathbf{y},p)-\frac{\tilde{k}(\mathbf{y})}{\tilde{E}(\mathbf{y})\tilde{\alpha}(\mathbf{y})}\overline{U}_j(\mathbf{x},\mathbf{y},p)\overline{q}^{(n)}(\mathbf{y},p)\right]d\Gamma-\overline{F}_j^{(n)(u)}(\mathbf{x},p)=0,\\
&\overline{\theta}^{(n)}(\mathbf{x},p)-\frac{\kappa_0\eta_0 p}{\gamma_0}\int_\Gamma\left[\overline{T}_i(\mathbf{x},\mathbf{y},p)\overline{u}_i^{(n)}(\mathbf{y},p)-\frac{1}{\tilde{E}(\mathbf{y})\tilde{\alpha}(\mathbf{y})}\overline{U}_i(\mathbf{x},\mathbf{y},p)\overline{t}_i^{(n)}(\mathbf{y},p)\right]d\Gamma\\
&\quad+\kappa_0\int_\Gamma\left[\overline{F}(\mathbf{x},\mathbf{y},p)\overline{\theta}^{(n)}(\mathbf{y},p)-\frac{\tilde{k}(\mathbf{y})}{\tilde{E}(\mathbf{y})\tilde{\alpha}(\mathbf{y})}\overline{T}(\mathbf{x},\mathbf{y},p)\overline{q}^{(n)}(\mathbf{y},p)\right]d\Gamma-\overline{F}^{(n)(\theta)}(\mathbf{x},p)=0,
\end{aligned}\tag{11}$$

where $\mathbf{x}$ and $\mathbf{y}$ represent the source and observation points, $\overline{U}_{ij}(\mathbf{x},\mathbf{y},p)$, $\overline{U}_i(\mathbf{x},\mathbf{y},p)$, $\overline{T}(\mathbf{x},\mathbf{y},p)$, $\overline{T}_{ij}(\mathbf{x},\mathbf{y},p)$, $\overline{T}_i(\mathbf{x},\mathbf{y},p)$, $\overline{Z}_i(\mathbf{x},\mathbf{y},p)$ and $\overline{F}(\mathbf{x},\mathbf{y},p)$ are the fundamental solutions [6, 8, 9]. Here, a tilde denotes the ratio of the non-homogeneous quantity to the corresponding homogeneous quantity. The functions $\overline{F}_j^{(1)(u)}$ and $\overline{F}^{(1)(\theta)}$ describe the non-homogeneity of the FG layer. They vanish completely for the homogeneous substrate $\Omega^{(0)}$. The functions $\overline{F}_j^{(1)(u)}$ and $\overline{F}^{(1)(\theta)}$ are defined as [8, 9]

$$\begin{aligned}
\overline{F}_j^{(1)(u)}(\mathbf{x},p)=&-p^2\int_\Omega\gamma^{(1)}(\mathbf{y})\overline{U}_{ij}(\mathbf{x},\mathbf{y},p)\overline{u}_i^{(1)}(\mathbf{y},p)d\Omega_y\\
&+\int_\Omega\left[\gamma_k^{(2)}(\mathbf{y})\overline{U}_{ij}(\mathbf{x},\mathbf{y},p)-\alpha^{(1)}(\mathbf{y})\overline{V}_{ijk}(\mathbf{x},\mathbf{y},p)\right]\overline{u}_{i,k}^{(1)}(\mathbf{y},p)d\Omega_y\\
&+\int_\Omega\left[p\eta^{(1)}(\mathbf{y})\overline{U}_j(\mathbf{x},\mathbf{y},p)-\gamma_j^{(3)}(\mathbf{y})\overline{U}_{kk}(\mathbf{x},\mathbf{y},p)\right]\overline{\theta}^{(1)}(\mathbf{y},p)d\Omega_y\\
&+\int_\Omega\left[\eta^{(2)}(\mathbf{y})\overline{E}_{ji}(\mathbf{x},\mathbf{y},p)-\gamma_i^{(4)}(\mathbf{y})\overline{U}_j(\mathbf{x},\mathbf{y},p)\right]\overline{\theta}_{,i}^{(1)}(\mathbf{y},p)d\Omega_y,
\end{aligned}\tag{12}$$

$$\begin{aligned}
\overline{F}^{(1)(\theta)}(\mathbf{x},p)=&\frac{\kappa_0\eta_0 p}{\gamma_0}\left\{p^2\int_\Omega\gamma^{(1)}(\mathbf{y})\overline{U}_i(\mathbf{x},\mathbf{y},p)\overline{u}_i^{(1)}(\mathbf{y},p)d\Omega_y\right.\\
&\left.-\int_\Omega\left[\gamma_k^{(2)}(\mathbf{y})\overline{U}_i(\mathbf{x},\mathbf{y},p)-\alpha^{(1)}(\mathbf{y})\overline{W}_{ik}(\mathbf{x},\mathbf{y},p)\right]\overline{u}_{i,k}^{(1)}(\mathbf{y},p)d\Omega_y\right\}\\
&-\int_\Omega\left[p\eta^{(1)}(\mathbf{y})\overline{T}(\mathbf{x},\mathbf{y},p)-\frac{\kappa_0\eta_0 p}{\gamma_0}\gamma_j^{(3)}(\mathbf{y})\overline{U}_j(\mathbf{x},\mathbf{y},p)\right]\overline{\theta}^{(1)}(\mathbf{y},p)d\Omega_y\\
&-\int_\Omega\left[\eta^{(2)}(\mathbf{y})\overline{G}_i(\mathbf{x},\mathbf{y},p)-\gamma_i^{(4)}(\mathbf{y})\overline{T}(\mathbf{x},\mathbf{y},p)\right]\overline{\theta}_{,i}^{(1)}(\mathbf{y},p)d\Omega_y,
\end{aligned}\tag{13}$$

where the fundamental solutions $\overline{E}_{ij}(\mathbf{x},\mathbf{y},p)$, $\overline{G}_i(\mathbf{x},\mathbf{y},p)$, $\overline{V}_{ijk}(\mathbf{x},\mathbf{y},p)$ and $\overline{W}_{ik}(\mathbf{x},\mathbf{y},p)$ are given in [8]. It should be noted that Eqs. (11) are no longer pure boundary integral formulations in the non-homogeneous sub-domain $\Omega^{(1)}$ because they involve domain integrals containing unknown fields. The BDIEs (11) contain boundary and domain integrals with singular kernels. The strongly singular integrals are interpreted in the sense of the Cauchy principal value. Making use of the

singularity subtraction technique and the variable transformation technique the strong and weak singularities in Eqs. (11) can be removed [2, 8, 9].

3. Numerical solution procedure

In order to avoid the domain discretization into internal cells for evaluating the domain integrals in Eqs. (12) and (13) the radial integration method (RIM) developed by Gao is applied [3, 4]. The functions (12) and (13) can be rewritten in matrix form [8] as

$$\bar{\mathbf{F}}(\mathbf{x}, p) = \int_{\Gamma} \bar{\mathbf{F}}(\mathbf{x}, \mathbf{y}, p)\bar{\mathbf{u}}(\mathbf{y}, p)d\Gamma + \int_{\Omega} \mathbf{G}(\mathbf{x}, \mathbf{y}, p)\bar{\mathbf{u}}(\mathbf{y}, p)d\Omega, \tag{14}$$

where $\bar{\mathbf{F}}$ is the vector of functions $\bar{F}_i^{(1)(u)}$ and $\bar{F}^{(1)(\theta)}$, $\bar{\mathbf{u}}$ is the vector containing the displacements $\bar{u}_i$ and the temperature $\bar{\theta}$, and the 3×3 matrices $\bar{\mathbf{F}}$ and $\bar{\mathbf{G}}$ are given in [8]. The unknown fields $\bar{u}_i$ or $\bar{\theta}$ are approximated by a series of prescribed basis functions and the linear polynomials

$$\bar{u}_i(\mathbf{x}, p) = \sum_A \bar{\alpha}_i^A(p)\phi^A(R) + \bar{a}_i^j(p)x_j + \bar{a}_i^0(p), \quad \sum_{A=1} \bar{\alpha}_i^A(p) = \sum_{A=1} \bar{\alpha}_i^A(p)x_j^A = 0, \tag{15}$$

where $R = \| \mathbf{x} - \mathbf{x}^A \|$ is the distance from the application point A to the field point $\mathbf{x}$, $\bar{\alpha}_i^A$ and $\bar{a}_i^j$ are the unknown expansion coefficients to be determined and x_j^A denotes the coordinates at the application point A, which consist of all boundary nodes and some selected internal nodes. The fourth order spline-type radial basis function [3, 4] is used

$$\phi^A(R) = 1 - 6R^2 + 8R^3 - 3R^4. \tag{16}$$

The unknown coefficients $\bar{\alpha}_i^A$ and $\bar{a}_i^j$ can be determined by applying the application point A in Eq. (16) to every node. Then, a system of linear algebraic equations can be obtained in matrix form as

$$\{\bar{u}\} = [\Phi]\{\bar{\alpha}\}, \tag{17}$$

where $\{\bar{\alpha}\}$ is the vector consisting of the coefficients $\bar{\alpha}_i^A$ for all points and $\bar{a}_i^j$. If two application points do not coincide, the matrix $[\Phi]$ is invertible and thereby

$$\{\bar{\alpha}\} = [\Phi]^{-1}\{\bar{u}\}. \tag{18}$$

Substitution of Eqs. (15) into the domain integrals of Eq. (14) yields

$$\int_{\Omega} \bar{G}_{ij}\bar{u}_j d\Omega = \bar{\alpha}_j^a \int_{\Omega} \bar{G}_{ij}\phi^a d\Omega + \bar{a}_j^k \int_{\Omega} \bar{G}_{ij} y_k d\Omega + \bar{a}_j^0 \int_{\Omega} \bar{G}_{ij} d\Omega. \tag{19}$$

Applying the RIM [3, 4, 8] to the domain integrals in Eq. (19) results in

$$\int_{\Omega} \bar{G}_{ij}\bar{u}_j d\Omega = \bar{\alpha}_j^a \int_{\Gamma} \frac{1}{r}\frac{\partial r}{\partial n}\bar{F}_{ij}^a d\Gamma + \bar{a}_j^k \int_{\Gamma} \frac{r_{,k}}{r}\frac{\partial r}{\partial n}\bar{F}_{ij}^1 d\Gamma + (\bar{a}_j^k x_k + \bar{a}_j^0)\int_{\Gamma} \frac{1}{r}\frac{\partial r}{\partial n}\bar{F}_{ij}^0 d\Gamma \tag{20}$$

with the radial integrals

$$\bar{F}_{ij}^a = \int_0^r r\bar{G}_{ij}\phi^a dr, \qquad \bar{F}_{ij}^1 = \int_0^r r^2\bar{G}_{ij} dr, \qquad \bar{F}_{ij}^0 = \int_0^r r\bar{G}_{ij} dr. \tag{21}$$

It is important to note here that the term $r_{,i}$ appearing in the radial integrals is constant [4] and the relation $y_k = x_k + r_{,k} r$ is used for the transformation from $\mathbf{y}$ to $\mathbf{r}$. The radial integrals (21) are regular and can be evaluated numerically by using standard Gaussian quadrature for every field point.

The BDIEs (11) can be solved numerically by applying a collocation method. The usual discretization procedure applied in BEM is utilized for the boundary discretization of the BDIEs in the Laplace-transformed domain [2, 6]. After numerical integrations, applying the prescribed boundary conditions and a rearrangement of the equations, a system of linear algebraic equations can be obtained as

$$\begin{array}{lllll} \mathbf{A}_0^b \mathbf{x}_0^b & = & \mathbf{y}_0^b, & \text{for boundary nodes,} & \text{for } \Omega_0, \\ \mathbf{A}_0^i \mathbf{x}_0^b + \mathbf{u}_0^i & = & \mathbf{y}_0^i, & \text{for internal nodes,} & \\ \mathbf{A}_1^b \mathbf{x}_1^b & = & \mathbf{y}_0^b + \mathbf{D}_1^b \mathbf{u}_1, & \text{for boundary nodes,} & \text{for } \Omega_1. \\ \mathbf{A}_1^i \mathbf{x}_1^b + \mathbf{u}_1^i & = & \mathbf{y}_0^i + \mathbf{D}_1^i \mathbf{u}_1, & \text{for internal nodes,} & \end{array} \tag{22}$$

Here, $\mathbf{x}_n^b$ is the $3N^b$ vector of the unknown values of the displacements $\bar{u}_i^{(n)}$, the tractions $\bar{t}_i^{(n)}$, the temperature $\bar{\theta}^{(n)}$ and the heat flux $\bar{q}^{(n)}$ at the boundary collocation points, $\mathbf{u}_n^i$ is the $3N^d$ vector of the unknown displacements $\bar{u}_i^{(n)}$ and temperature $\bar{\theta}^{(n)}$ at the internal nodes, $\mathbf{y}_n^b$ and $\mathbf{y}_n^i$ denote the $3N^b$ and $3N^d$ vectors composed of the prescribed boundary conditions. The sizes of the matrices $\mathbf{A}_n^b$, $\mathbf{A}_n^i$, $\mathbf{D}_1^b$ and $\mathbf{D}_1^i$ are $3N^b \times 3N^b$, $3N^d \times 3N^b$, $3N^b \times 3N$ and $3N^d \times 3N$, respectively, N^b and N^d are the numbers of boundary and internal nodes and $\mathbf{I}$ is the identity matrix. The system of linear algebraic equations (22) with the continuity conditions on the interface nodes (8) is solved numerically for discrete values of the Laplace-transform parameter p to obtain the boundary unknowns $\mathbf{x}_n^b$, the interior primary field quantities $\mathbf{u}_n^i$ and the unknown fields at the interface nodes [2]. The final time-dependent solutions can be calculated by using the Stehfest's algorithm [5] for the inverse Laplace-transform.

Different methods can be used for the evaluation of the SIFs. In this analysis, the extrapolation technique following directly from the asymptotic expansion of the displacements in the vicinity of the crack-tip is employed [2, 10]. For a crack located on the x_1-axis, the dynamic mode-I and mode-II SIFs are related to the crack-opening-displacements $\Delta u_i(\mathbf{x}, t)$ by

$$\begin{Bmatrix} K_{\mathrm{I}}(t) \\ K_{\mathrm{II}}(t) \end{Bmatrix} = \frac{\sqrt{2\pi}}{\kappa + 1} \mu^{\mathrm{tip}} \lim_{\varepsilon \to a} \frac{1}{\sqrt{a - \varepsilon}} \begin{Bmatrix} \Delta u_2(\varepsilon, t) \\ \Delta u_1(\varepsilon, t) \end{Bmatrix}, \tag{23}$$

where $\kappa = 3 - 4\nu_0$ or $\kappa = (3 - \nu_0)/(1 + \nu_0)$ for plane-strain or plane-stress conditions, respectively, μ^{tip} is the shear modulus at the crack-tip, and ε is a small distance from the crack-tip to the considered node on the crack-faces.

4. Numerical results

As a numerical example we consider an edge crack in a rectangular, isotropic and linear thermoelastic FG/homogeneous bimaterial plate, which is subjected to a cooling thermal shock $\theta(\mathbf{x}, t) = -\theta_0 H(t)$ as shown in Fig. 1a. Here, θ_0 is the constant loading amplitude and $H(t)$ is the Heaviside step function. The geometry of the cracked plate is determined by the width $w = 1$,

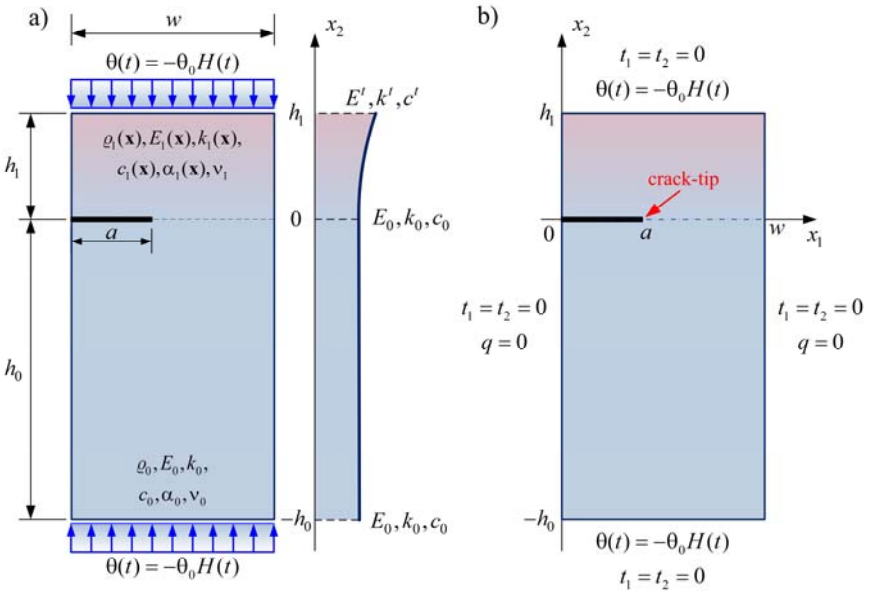

Figure 1. An edge crack in a FG/homogeneous bimaterial plate

height $h_0 + h_1 = 3w$ and crack-length $a = 0.4w$. An exponential material gradation with the gradient parameter α_g in the x_2-direction perpendicular to the crack-line of the FG coated structure is assumed as [8]

$$E = E_0 \exp(\alpha_g x_2), \qquad k = k_0 \exp(\alpha_g x_2), \qquad c = c_0 \exp(\alpha_g x_2). \tag{24}$$

The mass density, the Poisson's ratio and the linear thermal expansion coefficient are taken as $\tilde{\rho}(\mathbf{x}) = 1$, $\alpha(\mathbf{x}) = 0.02$ and $\nu = 0.25$, respectively. Plane-strain condition is assumed in the numerical calculations. The non-homogeneity of the FG layer induces a mixed mode crack-tip loading even though the cracked plate is subjected to a pure thermal loading on the top and the bottom side symmetric to the crack-faces, i.e., the mode-II dynamic SIF is also present along with the mode-I dynamic SIF. For convenience, the dynamic SIFs and the time are normalized as $\bar{K}_{I,II}(t) = K_{I,II}(t) / (\alpha_0 E_0 \theta_0 \sqrt{\pi a})$ and $\bar{t} = t\, k_0 / (a^2 \tilde{\rho}_0 c_0)$.

To test the accuracy of the proposed BEM, the numerical results are compared with those obtained by the FEM analysis, which show a good agreement [8, 9, 11]. The time variations of the normalized mode-I and mode-II SIFs for the three selected combinations of the gradient parameters $\alpha_g h_1 = \ln(2),\ \ln(3),\ \ln(5)$ and $\alpha_g h_1 = \ln(0.5),\ \ln(0.333),\ \ln(0.2)$ are presented in Figs. 2 and 3. The negative gradient parameters (Fig. 3) result in a reduction of the peak dynamic SIFs in comparison to that for positive gradient parameters (Fig. 2). The wave velocity in this case is also decreasing. Hence, the peak values of the dynamic SIFs are reached at larger time instants. The opposite tendency is observed in Fig. 2 with the increasing gradient parameters. Thus, the present results show that the gradient parameters may have significant influences on the dynamic SIFs. To investigate the influence of the thickness of the FG coating on the dynamic SIFs, four relative thickness values $h_0 / h_1 = 5,\ 10,\ 15,\ 20$ are selected for the gradient parameters $\alpha_g h_1 = \ln(2)$ and $\alpha_g h_1 = \ln(0.5)$ in the numerical analysis. The time variations of the normalized mode-I and mode-II dynamic SIFs for the selected thickness ratios are shown in Figs. 4 and 5. The peak of the SIFs decreases with decreasing thickness of the FG layer for both values of the material gradient parameter.

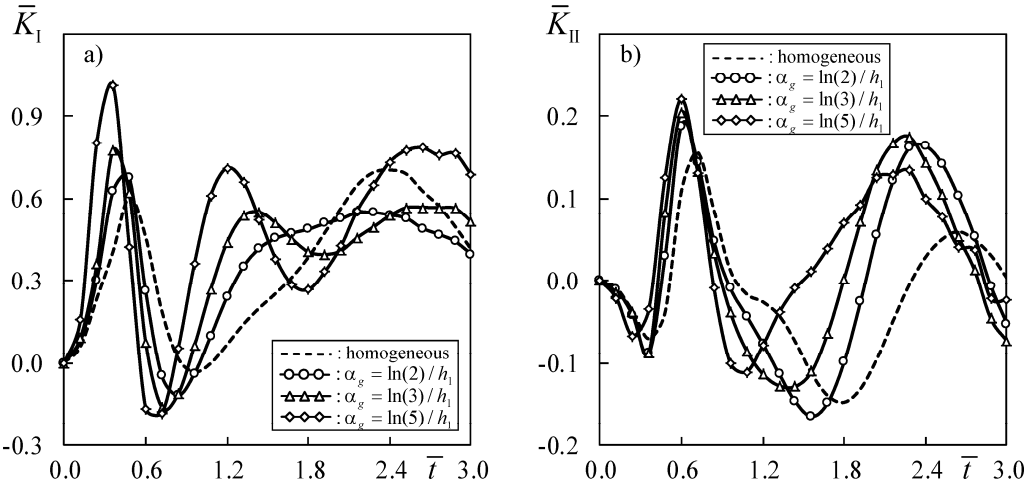

Figure 2. Normalized dynamic a) mode-I and b) mode-II SIFs for $\alpha_g h_1 = \ln(2), \ln(3), \ln(5)$

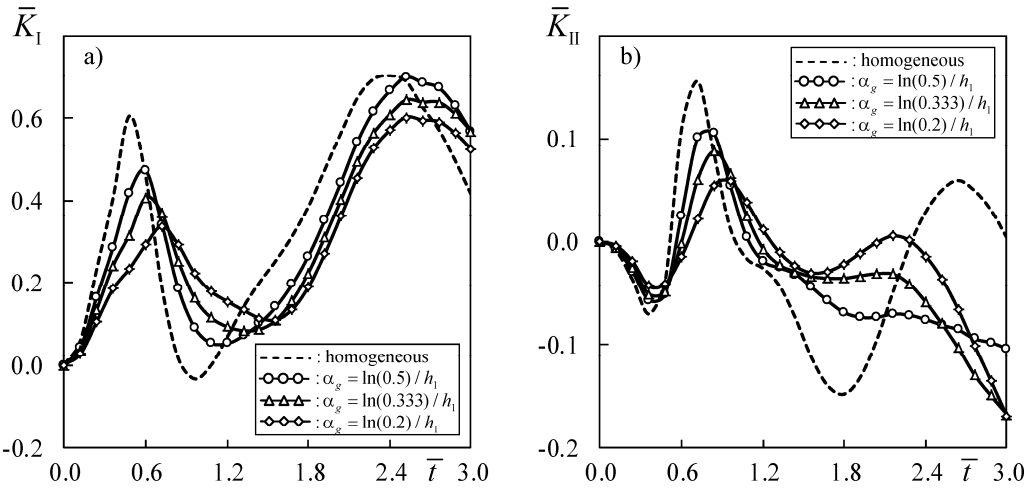

Figure 3. Normalized dynamic a) mode-I and b) mode-II SIFs for $\alpha_g h_1 = \ln(0.5), \ln(0.333), \ln(0.2)$

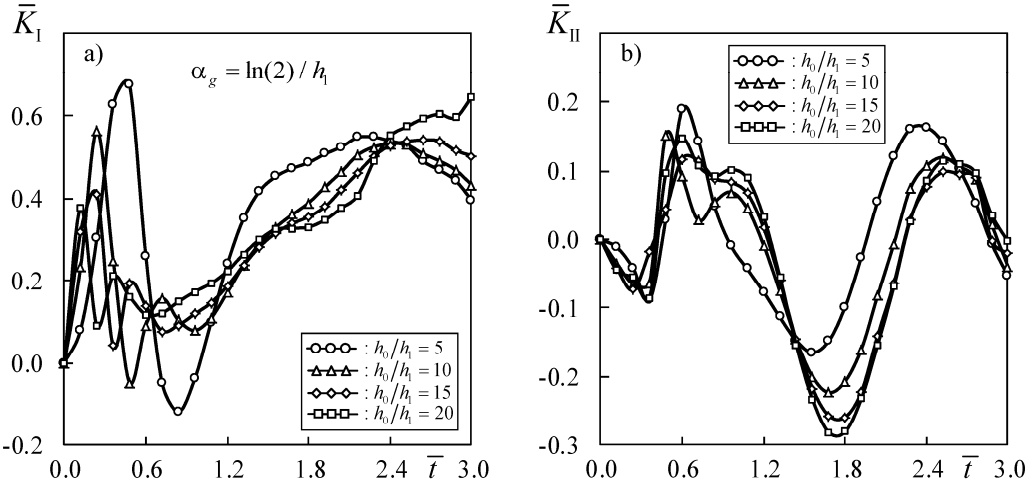

Figure 4. Normalized dynamic a) mode-I and b) mode-II SIFs for $h_0/h_1 = 5, 10, 15, 20$ and $\alpha_g h_1 = \ln(2)$

The effects of the thermo-mechanical coupling on the normalized dynamic mode-I and mode-II SIFs can be observed in Figs. 6 and 7. In this case, the thermo-mechanical coupling parameter (5) is taken as $\delta = 0.133$ and $\delta = 0.3$, which correspond to the previously used material parameters with the reference temperatures $T_0 = 100$ and $T_0 = 225$, respectively. With the increase of the coupling

parameter, the peak values of the normalized dynamic SIFs are reduced. The numerical results imply that the maximum amplitudes of the normalized dynamic SIFs and the time instants, at which they occur, depend significantly on the values of the gradient parameters, the ratios of the thicknesses and the thermo-mechanical coupling.

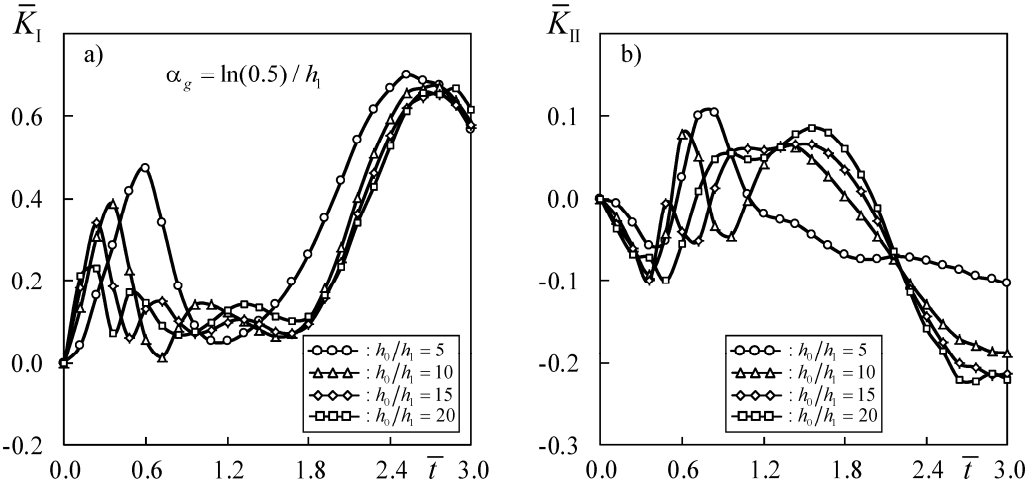

Figure 5. Normalized dynamic a) mode-I and b) mode-II SIFs for $h_0 / h_1 = 5,10,15,20$ and $\alpha_g h_1 = \ln(0.5)$

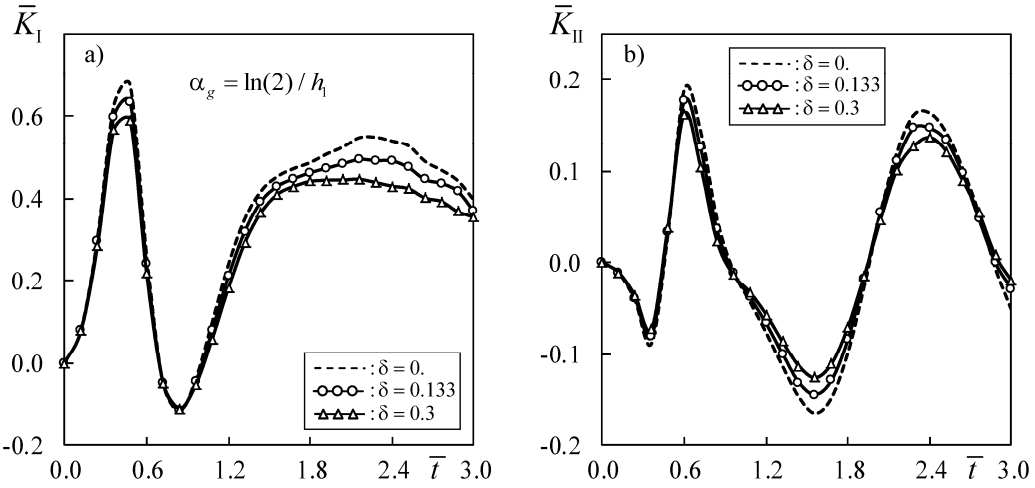

Figure 6. Normalized dynamic a) mode-I and b) mode-II SIFs for $\delta = 0, 0.133, 0.3$

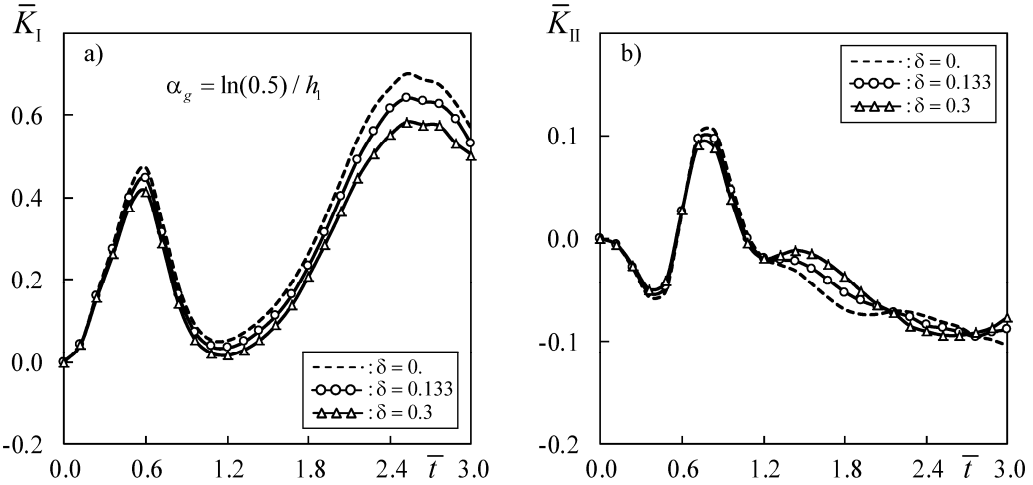

Figure 7. Normalized dynamic a) mode-I and b) mode-II SIFs for $\delta = 0, 0.133, 0.3$

5. Summary

A BEM for 2-D transient coupled thermoelastic crack analysis in FG/homogeneous bimaterials under thermal shock is presented in this paper. The sub-domain technique is applied to model the FG/homogeneous bimaterials. Fundamental solutions of linear coupled thermoelasticity for homogeneous, isotropic and linear thermoelastic solids are used to derive the boundary-domain integral equations. The material non-homogeneity of the FG layer is described by domain integrals, which are evaluated by using the RIM. A collocation-based BEM is developed in the Laplace-transformed domain. The numerical inversion of the Laplace-transform is performed by Stehfest's algorithm. The dynamic SIFs are evaluated by using displacement extrapolation technique. The temporal variations of the dynamic SIFs for an edge crack in a 2-D FG/homogeneous bimaterial plate are presented. The effects of the material gradation, the FG coating thickness and the thermo-mechanical coupling on the dynamic SIFs are analyzed.

Acknowledgement

This work is supported by the German Research Foundation (DFG, Project-No.: ZH 15/10-2), which is gratefully acknowledged.

References

[1] S. Suresh and A. Mortensen, Fundamentals of functionally graded materials: Processing and thermomechanical behaviour of graded metals and metal-ceramic composites. IOM Communications Ltd, London, 1998.

[2] L. C. Wrobel and M. H. Aliabadi, The boundary element method. J. Wiley, Chichester, New York, 2002.

[3] X. W. Gao, The radial integration method for evaluation of domain integrals with boundary-only discretization. Eng Anal Boundary Elem, 26 (2002) 905-916.

[4] X. W. Gao, A boundary element method without internal cells for two-dimensional and three-dimensional elastoplastic problems. J Appl Mech, 69 (2002) 154-160.

[5] H. Stehfest, Numerical Inversion of Laplace Transforms. Commun ACM, 13 (1970) 47-49.

[6] J. Balaš, J. Sládek and V. Sládek, Stress analysis by boundary element methods. Elsevier, Amsterdam, New York, 1989.

[7] J. Sladek, V. Sladek, C. Zhang and C. L. Tan, Meshless local Petrov-Galerkin method for linear coupled thermoelastic analysis. Comp Model Eng Sci, 16 (2006) 57-68.

[8] A. Ekhlakov, O. Khay, C. Zhang, J. Sladek, V. Sladek and X. W. Gao, Thermoelastic crack analysis in functionally graded materials and structures by a BEM. Fatigue & Fract of Eng Mater & Struct, 35 (2012) 742-766.

[9] A. V. Ekhlakov, O. M. Khay, C. Zhang, J. Sladek and V. Sladek, A BDEM for transient thermoelastic crack problems in functionally graded materials under thermal shock. Comput Mater Sci, 57 (2012) 30-37.

[10] J. Sladek, V. Sladek and C. Z. Zhang, An advanced numerical method for computing elastodynamic fracture parameters in functionally graded materials. Comput Mater Sci, 32 (2005) 532-543.

[11] A. V. Ekhlakov, O. M. Khay, C. Zhang, J. Sladek and V. Sladek, Transient coupled thermoelastic crack analysis in functionally graded materials. Struct Durab Health Monitor, 6 (2010) 329-350.